Coastal Dynamics 2017
Paper No. 172

EFFECT OF TIME HISTORY OF VELOCITY ON INSTANTANEOUS SEDIMENT TRANSPORT IN THE SWASH ZONE

Lianhui Wu[1], Dejun Feng[2], and Akio Okayasu[3]

Abstract

A laboratory experimental study for sediment transport in the swash zone was carried out by using dambreak flow. Sediment concentration and transport velocity were measured by a light distinction method and particle image velocimetry respectively. Sediment flux was quantified by the product of aforementioned two factors for the whole swash event with a vertical resolution of 0.27 mm. The data were used to investigate the effect of velocity history on instantaneous sediment transport and two empirical sediment transport models were compared. It was found that except for the early uprush and late backwash, instantaneous depth-averaged sediment flux decayed following the decreasing velocity with a relatively stable rate. Neither Bagnold's energetics model nor Shields parameter model showed satisfying predictive ability in the swash zone. Failure of these models was considered to be resulted from significant sediment advection and turbulence.

Key words: swash zone, sediment flux, empirical sediment transport model, PIV, image analysis

1. Introduction

The swash zone is an active region connecting the inner surf zone and coastal land. Due to its thin water depth, complex flow structure and large amount of sediment transport, direct measurement of the swash zone is very difficult. Even though many research efforts have been made to improve our knowledge of this challenging region, understanding of this zone is still far away from satisfactory (Chardón-Maldonado et al., 2016).

Understanding of the swash zone processes is fundamental to predict beach erosion and accretion (Briganti et al., 2016). Recent studies of swash zone sediment transport aimed at improving the capability to achieve quantitatively accurate predictions of bed profile evolution. A key factor is how to couple sediment transport with hydrodynamics. Phase resolving wave models are often coupled with sediment transport models based on energetics type formulations (e.g. Bagnold, 1963, 1966; Meyer-Peter and Müller, 1948). A few recent studies have shown that this approach has moderate accuracy (Masselink et al., 2005; Othman et al., 2014) while lots of researches indicated that its applicability in the swash zone is limited (Aagaard and Hughes, 2006; Butt et al., 2005). Since these energetics models are initially developed for steady, unidirectional flow, poor applicability in the swash zone is not surprising. On the other hand, incomplete sampling of the entire swash event and low vertical resolution made the real predictive ability of these energetics type models questionable (Chardón-Maldonado et al., 2016).

Wu et al. (2014) developed a new image-based measurement method for sediment flux with high resolution and it has been utilized to measure sediment transport in the swash zone successfully (Wu et al., 2016). They have published experimental results of sediment flux and bed level evolution and confirmed that the difference between the measured net sediment load and bed level change is small, indicating the reliability and accuracy of the measurement. In this paper, we focus on the effect of the time history of

[1] Graduate School of Marine Science and Technology, Tokyo University of Marine Science and Technology, 4-5-7, Konan, Minato-ku, Tokyo 108-0075, Japan. d142018@edu.kaiyodai.ac.jp
[2] Graduate School of Marine Science and Technology, Tokyo University of Marine Science and Technology, 4-5-7, Konan, Minato-ku, Tokyo 108-0075, Japan. d132016@edu.kaiyodai.ac.jp
[3] Department of Ocean Sciences, Tokyo University of Marine Science and Technology, 4-5-7, Konan, Minato-ku, Tokyo 108-0075, Japan. okayasu@kaiyodai.ac.jp

velocity on the instantaneous sediment transport and the applicability of the energetics type models in the swash zone based on the high-resolution data.

2. Description of the experiment

2.1. Experimental set-up

The experiment was carried out in a modified open channel flume (7.1 m long, 0.3 m wide and 0.7 m high) (Fig. 1). A reservoir was placed at one end of the glass-sided flume. The reservoir was fronted by a steel gate, which could be lifted rapidly to generate a single dambreak bore propagating toward a sloping beach. The sandy beach was built on a 1:6 fixed slope. The median diameter (d_{50}) of the sand used in the experiments was 0.16 mm. In the experiment, the reservoir was filled with water to a depth of 20.0 cm, and the water depth in front of the gate was set at 2.0 cm. The dambreak swash run was repeated for 20 times without restoring the sandy beach after each swash event. A swash run consisted of the dambreak flow running up and down over the sandy beach without any swash-swash interaction. Therefore, the swash run represents a 'pure' swash event. For each run, the gate was lifted by hands to generate a swash flow and water in the flume was pumped back to the reservoir for the next swash run. The origin of the x - z coordinate system was located at the toe of the sandy beach, with the x-axis directed shoreward along the initial beach surface, and the z-axis perpendicular to the beach surface (z = 0 was the initial bed level in the measurement position before the first run). More details of the experiment could be found in Wu et at. (2016).

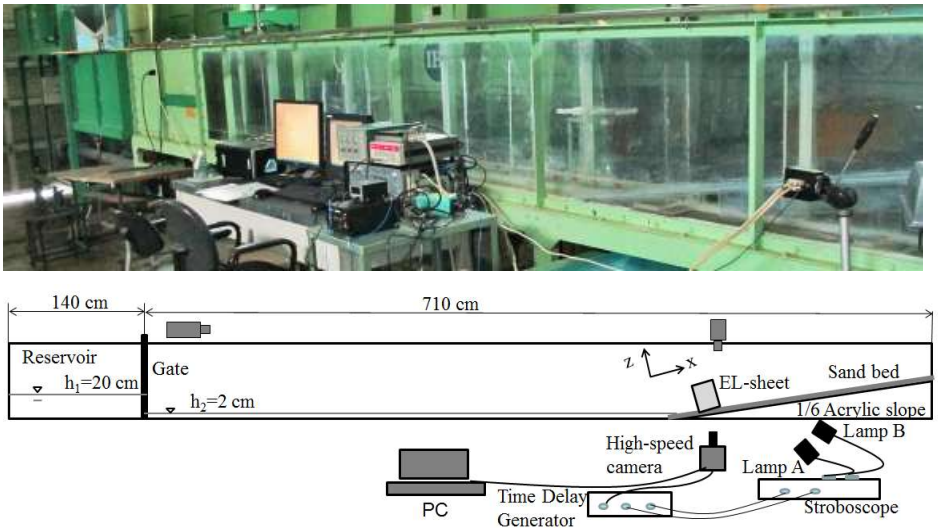

Figure 1. Modified open channel flume and experimental set-up

2.2. Instruments and methodology

Intra-swash sediment flux (instantaneous sediment flux within a swash event) was obtained from sediment concentration and sediment transport velocity measured by an image-based technique. Sediment concentration was measured by a light extinction method using a backlight source and sediment transport velocity was measured by particle image velocimetry (PIV).

An electro-luminance sheet (20 cm long, 15 cm high, and 0.07 cm thick; El-sheet hereafter) was placed in the swash flow parallel to the flume side-walls at 30 cm from the toe of the sandy beach as a backlight source. The El-sheet, a near-homogeneous planar light sheet with a brightness of 100 cd/m^2, was installed 1.5 cm inside from the front side wall. The El-sheet was fixed to the acrylic bottom plate so that sand under

the initial bed level was able to be illuminated. The thickness of the EL-sheet was so thin that the influence of the sheet to the flow was limited. A high-speed camera (IDT Inc., M3) with a Nikon lens of fixed 50 mm focal length was focused on the EL-sheet to record the sediment movement in front of the EL-sheet. It was rotated to be aligned to the initial sandy beach and fixed at 30 cm away from the El-sheet to give a resolution of 66 μm/pixel. The rate of the high-speed camera was set at 1000 frames per second (fps). The size of the recorded images was 520 × 1000 pixels, corresponding to a field of view (FOV) of 3.47 cm × 6.67 cm captured area. The high-speed camera was triggered when the flow reached the toe of the beach and $t = 0$ was defined as the flow firstly appeared in the recorded area. According to the Beer-Lambert law, light brightness of the El-sheet would be attenuated by the emergence of the sandy flow and the rate of attenuation (A) has a linear relationship with the sand concentration (c) in front of the El-sheet,

$$A = log\frac{B}{B_0} = k$$

where B and B_0 are light brightness with and without sandy flow in front of the El-sheet, respectively. k is a coefficient which was determined by a pre-calibration test. Since the light brightness could be measured from the recorded images, sediment concentration could be calculated from the light attenuation rate at every pixel of the images.

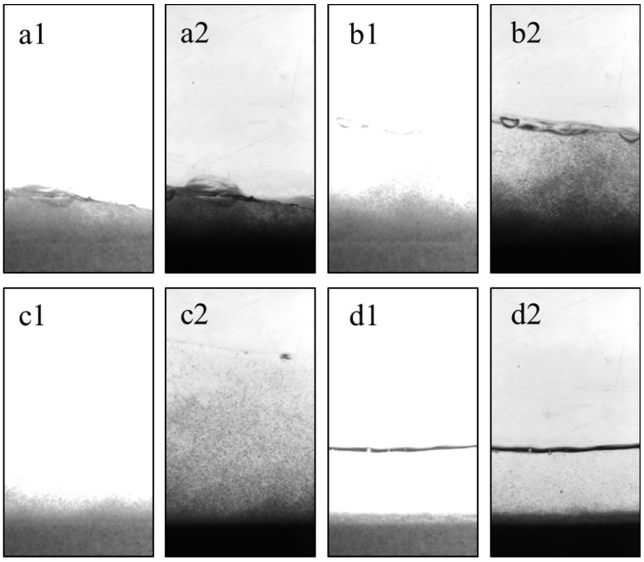

Figure 2. Contiguous combined and single illuminated images of initial uprush (a), middle uprush (b), flow reversal (c) and late backwash (d), time interval between 2 images of every pair is 0.001 s.

Different from the conventional PIV with a laser system illuminating the seeded tracer particles, sand particles were directly used as tracer particles with the El-sheet as the light source in this study. In addition, a dual lamp stroboscope system (Nissin Electronic Corporation, SA-100B-W) was employed as an additional light source when the sediment concentration was too high to be illuminated by the El-sheet. The stroboscope was synchronized with the high-speed camera by a digital delay generator (Stanford Research Systems, Inc., DG645) with a frequency of 100 Hz which was one tenth of the camera frequency. The delay generator gave one signal to each of the two lamps in one cycle and time difference between the two signals was set at 0.001 s. Therefore, 2 successive images which were combined-illuminated by the El-sheet and the stroboscope and 8 images which were single-illuminated by the El-sheet were obtained within every cycle of 0.01 s. Contiguous couples of combined- and single-illuminated images for different swash phases are shown in Fig. 2. Highly concentrated sand in the vicinity of the bed could be clearly illuminated by the stroboscope, especially in the early uprush. Therefore, transport velocity close to the bed was obtained from the combined-illuminated images, incorporating with the velocities obtained from the

single illuminated images in the upper layer; intra-swash transport velocity field was obtained at 100 Hz. An FFT-based multiple-pass cross-correlation algorithm with a grid refining scheme was adopted to measure the velocity field (Raffel et al., 2007). Two iterations of cross-correlation with interrogation windows of 96 × 32 pixels and 96 × 16 pixels were carried out to estimate integer displacement. A parabolic curve fitting function was employed to obtain sub-pixel accuracy (Raffel et al., 2007). The distance between two adjacent measurement points in the z-direction was 4 pixels (0.27 mm) leading to a vertical overlap of 75%. Ten inspection lines (marked from left to right) with an adjacent distance of 40 pixels in the cross-shore direction were selected to estimate the velocity field. A detailed description of the measurement methodology could be found in Wu et al. (2014).

3. Instantaneous sediment transport

Examples of velocity and concentration fields at representative phases for uprush and backwash are shown in Fig. 3. Sediment concentration was obtained from light attenuation averaged over the same interrogation window as in the second iteration of PIV analysis. Thus, sediment concentration and transport velocity of the same spatial resolution were measured to calculate bed-parallel sediment transport rate (sediment flux) as a product of the two quantities:

$$q = uc$$

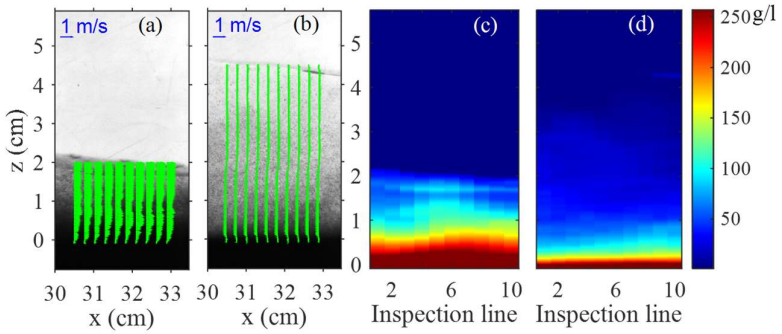

Figure 3. Examples of velocity (a, b) and concentration (c, d) fields in the uprush (a, c) and flow reversal (b, d), (color bar indicates the scale of sediment concentration; horizontal axis of concentration field is the index of inspection line corresponding to the velocity field.

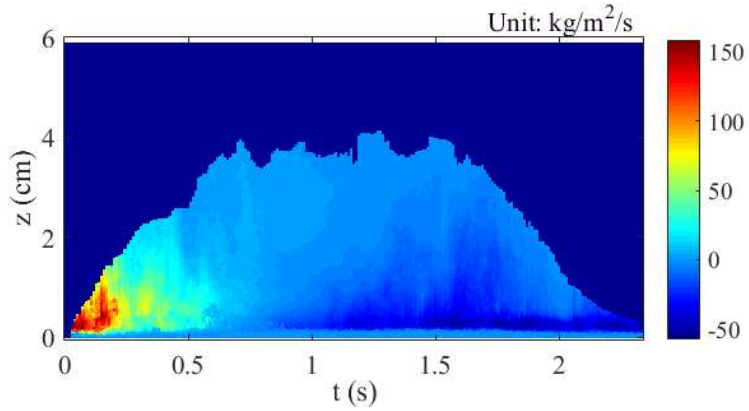

Figure 4. Temporal and spatial behavior of instantaneous sediment flux measured at inspection line 5 within a swash period.

where q is the instantaneous horizontal sediment flux, u is the instantaneous bed parallel transport velocity. Data quality control was carried out to improve the measurement reliability and accuracy. Measurement error mainly stemmed from the air bubbles and the uneven water surface. Either concentration or velocity measurement was likely to be influenced. Hence, suspicious data close to the water surface were removed based on a local median filter (Raffel et al., 2007). Note that sediment concentration in the vicinity of the water surface was relatively low and this data quality control gave little effect on the quantification of sediment transport.

Fig. 4 shows the temporal and spatial behavior of sediment flux measured at inspection line 5 within a swash period. It is the first time that the instantaneous sediment fluxes are plotted against the velocities in the swash zone for an entire swash period attributing to the unique measurement method. Significant sediment fluxes were observed during the initial uprush. Sediment advection from the lower swash zone greatly contributed to the sediment flux at the measurement location. Since sediment concentration in the backwash was much weaker than that in the uprush, magnitude of maximum offshore sediment flux (-56 kg/m^2/s) was only about 1/3 of the maximum onshore sediment flux (150 kg/m^2/s). Because of the low transport velocity (within the bottom boundary layer), sediment fluxes in the vicinity of the bed were very small even though the concentration is much higher. On the other hand, sediment flux in the upper layer was also small resulted from the very low concentrations even though the transport velocity was large there.

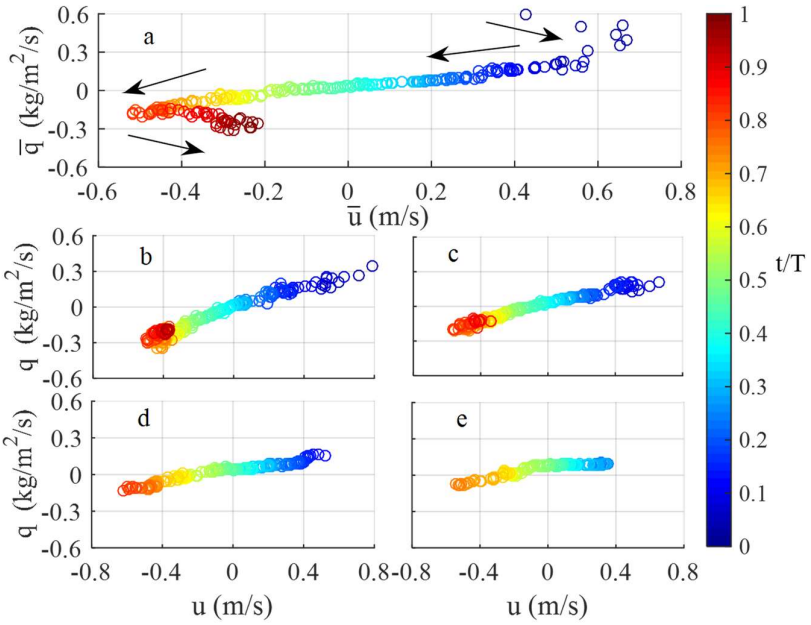

Figure 5. Scatter plot of instantaneous horizontal velocity and sediment flux measured at inspection line 5 within a swash period, a: depth-averaged; b: z = 0.5 cm; c: z = 1 cm; d: z = 2 cm; e: z = 3 cm; color bar indicates the time normalized by swash event period T.

Scatter plots of instantaneous depth-averaged horizontal velocity and depth-averaged sediment flux measured at inspection line 5 within a swash period were shown in Fig. 5. It is found that except for the early uprush and late backwash, instantaneous depth-averaged sediment flux decayed following the decreasing velocity with a relatively stable rate. In the late backwash, due to sediment resuspension, although transport velocity declined but the magnitude of instantaneous depth-averaged (negative) sediment flux increased. Instantaneous sediment flux at high elevation showed a monotonous tendency with horizontal velocity (Figure 5d, e). Variation rate decreased with the elevation since the concentrations are much smaller in the upper layers while velocities varied little within the water column (except for the bottom boundary layer). It is considered that reversions in the uprush and backwash are due to bore related

and bed related turbulence, respectively. Therefore, in order to precisely predict sediment transport in the swash zone, turbulence and advection processes are necessary to be taken into account in numerical models.

4. Empirical sediment transport models

Most of the models for cross-shore swash zone sediment transport are based on either Bagnold (1963; 1966) energetics approach or Shields parameter type model (Meyer-Peter and Müller, 1948) even though these models are initially developed for steady flow. Comparison between field data and modeling results ranges from very poor, with an incorrect net transport direction, to uncertain. One reason should be that in the most of the previous studies instantaneous sediment flux was evaluated by multiplying estimated sediment concentration and velocity at a single elevation. A previous study has shown that only using velocity at one elevation would underestimate total sediment flux (Masselink et al., 2005). It is suggested that sediment flux with high spatial and temporal resolution is required in order to further examine these empirical sediment transport model. Therefore, based on the high-resolution data of present experiment, we investigated the applicability of these empirical sediment transport model in the swash zone.

4.1. Bagnold's model

Bagnold's energetics type models are based on the assumption that a part of the fluid power (ω) is able to be delivered to the sediment particles and initiate their mobilization. The Bagnold's bed load and suspended load models are described as:

$$I_b = \frac{k_b \omega}{tan\varphi - tan\beta}$$

$$I_s = \frac{0.5(1 - k_s)\omega}{W/u_s - (|u|/u)tan\beta}$$

where, I_b and I_s are immersed weight of bed load and suspended load, respectively. k_b and k_s are bed load and suspended load coefficient (kg/m^3), respectively. φ is the internal friction angle of the sediment ($\tan\varphi = 0.63$), β is the bed slope, W is the sediment fall velocity and u_s is the horizontal velocity of the sediments. The fluid power is often related to the product of free stream velocity and bed shear stress ($\omega = u\tau$).

Many past studies have evaluated the Bagnold's energetics models by using field measurements of swash zone sediment flux. Bed shear stress is often described in the form $\tau = 0.5\rho f u|u|$ and an empirical constant f is usually adopted in the past studies for calibrating the Bagnold's energetics approach. Thus, the Bagnold's energetics models can be simplified to $I_b = k_b u^3$ and $I_s = k_s u^4$ if the sediment velocity is assumed to be equal to the fluid velocity. These type of Bagnold's energetics models have been calibrated either in the inter-swash time scale over individual wave circles or half circles usually by use of sediment traps (Hardisty et al., 1984; Hughes et al., 1997; Masselink and Hughes, 1998; Masselink et al., 2009) or in intra-swash time scale relying on the collaborated measurements of sediment concentration and transport velocity (Puleo et al, 2000). The calibration of Bagnold's energetics models shows varying degrees of success (Butt et al., 2005). A common finding is that the coefficient of uprush is greater than that of backwash, suggesting that uprush is more powerful to transport sediments.

In this study, in order to evaluate the applicability of the Bagnold's energetics approach for intra-swash sediment transport, instantaneous parameters of depth-averaged sediment flux and the product of bed shear stress and depth averaged velocity are used as inputs.

Bed shear stress was calculated from von Karman-Prandtl's logarithmic model,

$$u(z) = \frac{u_*}{\kappa} ln(\frac{z - 0.7d_{50}}{z_0})$$

$$\tau = \rho u_*^2$$

where u_* is the friction velocity, κ is the von Karman's constant (0.4), z_0 is the height above the bed at which velocity is assumed to be zero. z_0 equals to $k_s/30$, where k_s is the equivalent Nikuradse roughness. τ is bed shear stress, ρ is the fluid density. Shear velocity was estimated from a least square regression using same with previous studies (Cox et al., 1996; Puleo et al., 2012).

The velocity of sand and fluid are assumed to be identical. W is calculated by (Soulby, 1997),

$$W = \frac{\mu}{\rho d_{50}}\left(\sqrt{1.049 d_*^3 + 107.3} - 10.36\right)$$

$$d_* = d_{50}\left[\frac{\rho^2 g(s-1)}{\mu^2}\right]^{1/3}$$

where $\mu = 10^{-3}$ Ns/m is the dynamic viscosity of the fluid, d_* is the dimensionless grain size, $s = 2.65$ is the specific gravity of the sediment and g is the gravitational acceleration.

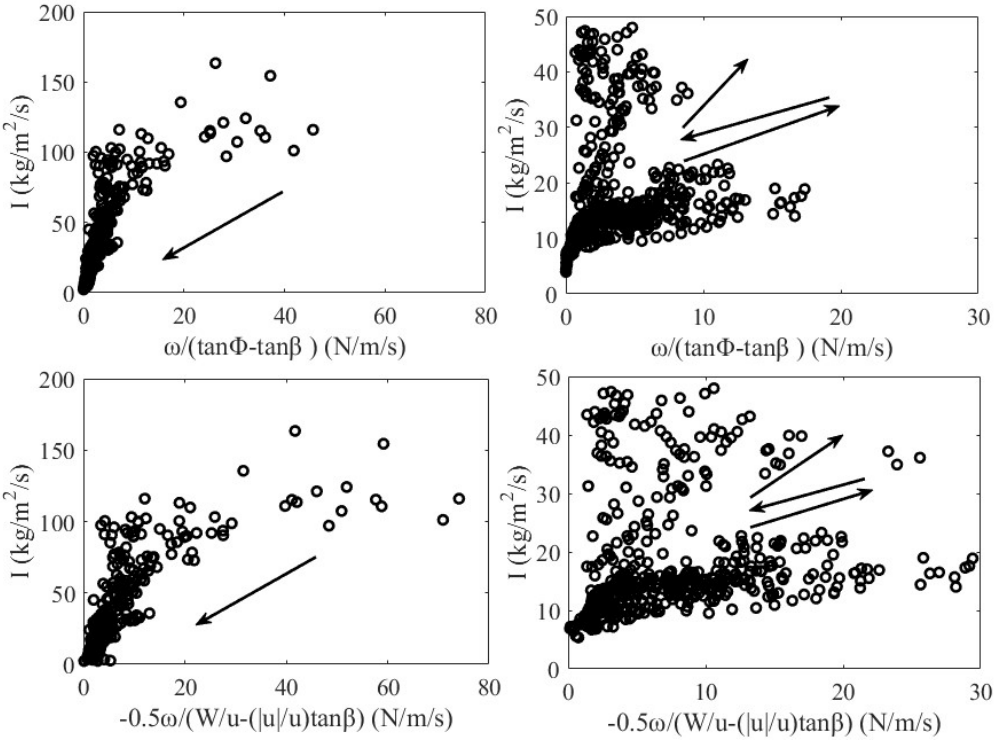

Figure 6. Intra-swash comparison between Bagnold's energetics approach and the instantaneous depth averaged sediment fluxes of 4 swash runs. Bed load model for uprush (upper left panel), bed load model for downwash (upper right panel), suspended load model for uprush (lower left panel) and suspended load model for downwash (lower right panel), arrows indicate the temporal sequence of data points.

Fig. 6 shows the comparison between the Bagnold's energetics models and the instantaneous depth averaged sediment flux of 4 swash runs. Arrows in the figure indicated the temporal sequence of the data points. Instantaneous depth averaged sediment fluxes showed a monotonous decreasing tendency during the uprush. And a linear relationship could be inferred both for the bed load and suspended load model apart from the initial uprush, where depth averaged sediment flux was relatively large. Failure in the initial uprush might be stemmed from the bore-generated turbulence and sediment advection. Depth averaged

sediment flux kept growing after the flow reversed to offshore. Both the magnitudes of bed shear stress and depth-averaged transport velocity were enhancing during the former half backwash, resulting in an increase in the fluid power. Correspondingly, a linear relationship was observed before the peak of offshore velocity. Bed shear stress and depth-averaged transport velocity started to decay after the peak of offshore velocity and it increased strongly in the late backwash, making the fluid power became disorder relating to the instantaneous depth averaged sediment flux. Based on the current experimental results, Bagnold's energetics approach seems to be more reliable during uprush than backwash but it is not completely adequate for predicting sediment transport in the swash zone as has been demonstrated by many other researchers (Butt et al., 2005; Puleo et al., 2005; Blenkinsopp et al., 2011) and the suspended load model shows no advantage over the bed load model.

4.2. Meyer-Peter and Müller's model

The Shields parameter type model was also validated by using the measured data of this study. Meyer-Peter and Müller (1948) suggested the non-dimensional sediment transport rate Φ has a relationship with the Shields parameter as following,

$$\Phi = k_c(\theta - \theta_c)\sqrt{\theta}$$

where Φ and θ are respectively defined as

$$\theta = \frac{\tau}{\rho(s-1)gd_{50}}$$

$$\Phi = \frac{I}{d_{50}\sqrt{(s-1)gd_{50}}}$$

k_c is an empirical coefficient (k_c = 12; Nielsen, 1992), and θ_c is the critical Shields stress parameter below which no sediment transport occurs ($\theta_c = 0.05$). Fig. 7 presents the comparison of measured and modeled intra-swash non-dimensional sediment transport rate of two swash runs. The model is only capable of predicting the general tendency of the sediment transport rate but shows poor agreement in the magnitudes. O'Donoghue et al. (2016) also tested the Shields type model, and found a factor of 2 in the difference between the measured and modeled transport rate. One probable reason is that sediments used in their experiments are much coarser (d_{50} = 1.3 mm and 8.4 mm), so sediment advection might be much weaker than the present study.

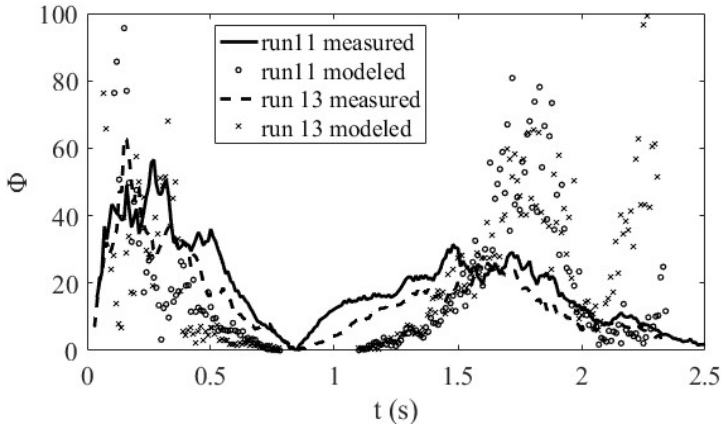

Figure 7. Comparison of measured and modeled intra-swash non-dimensional sediment transport rate.

5. **Conclusions**

A laboratory experiment was carried out on a mobile fine sandy beach. Intra-swash sediment transport was captured throughout the entire swash runs including the initial uprush and late backwash. Sediment concentration was measured by a light extinction method and transport velocity was measured by PIV. Sediment flux was quantified by the products of the two factors with high temporal and spatial resolution. Effect of velocity history on instantaneous sediment transport was investigated and applicability of two empirical sediment transport models in the swash zone was tested by using present experimental data. The following are the main conclusions of this study:

1) Sediment advection from the lower swash zone greatly contributed to the sediment flux at the measurement location. The magnitude of maximum offshore sediment flux was only about 1/3 of the maximum onshore sediment flux at the measurement location.
2) Except for the early uprush and late backwash, instantaneous depth-averaged sediment flux decayed following the decreasing velocity with a relatively stable rate. In the late backwash, due to sediment resuspension, transport velocity declined but the magnitude of instantaneous depth-averaged (negative) sediment flux increased.
3) Instantaneous sediment flux at high elevation showed a monotonous tendency with horizontal velocity. Variation rate decreased with the elevation since the concentrations are much smaller in the upper layers while velocities varied little within the water column (except for the bottom boundary layer).
4) In the uprush, a linear relationship between sediment transport rate and fluid power could be inferred either for the Bagnold's bed load or suspended load model apart from the initial stage. Failure in the initial uprush was suggested due to the bore-generated turbulence and sediment advection. In the backwash, a linear relationship was also observed before the peak of offshore velocity. It is suggested that because of the change of bed shear stress, models failed in the later backwash.
5) The Shields parameter model can only predict the general tendency of instantaneous sediment transport, which is considered to be resulted from serious sediment advection since fine sand was used in present study.

The present study is a first step for improving the predictive ability of sediment transport in the swash zone. Further studies of sediment pick-up are undergoing in order to understand the entrainment process of sand in the swash zone.

Acknowledgements

A part of this study was supported by JSPS KAKENHI Grant Numbers 26289161.

References

Aagaard, T., Hughes, M.G., 2006. Sediment suspension and turbulence in the swash zone of dissipative beaches. *Mar. Geol.*, 228 (1–4), 117–135.

Bagnold, R. A., 1963. *Mechanics of marine sedimentation.* The sea, Hill, M. N. (editor), Vol. 3, Wiley Interscience, New York.

Bagnold, R. A., 1966. An approach to the sediment transport problem from general physics. No. 422-I, US Geological Survey, Washington, DC.

Blenkinsopp, C.E., Masselink, G., Turner, I.L., Russell, P.E., 2011. Can standard energetics models be used to predict net cross-shore sediment flux at the beach face? *Australian J. of Civil Eng.*, 9 (1), 19-34.

Briganti, R., Torres-Freyermuth, A., Baldock, T.E., Brocchini, M., Dodd, N., Hsu, T.J., Jiang, Z., Kim, Y., Pintado-Patino, J.C., Postacchini, M., 2016. Advances in numerical modeling of swash zone dynamics. *Coas. Eng.*, 115, 26–41.

Butt, T., Russell, P., Puleo, J.A., Masselink, G., 2005. The application of Bagnold-type sediment transport models in

the swash zone. *Cont. Shelf Res*., 21, 887–895.
Chardón-Maldonado, P., Pintado-Patino, J.C., Puleo, J.A., 2016. Advances in swash-zone research: small-scale hydrodynamic and sediment transport processes. *Coast. Eng.*, 115, 8-25.
Cox, D.T., Kobayashi, N., Okayasu, A., 1996. Bottom shear stress in the surf zone. *J. Geophys. Res.: Oceans*, 101 (C6), 14337–14348.
Hardisty, J., Collier, J., Hamilton, D., 1984. A calibration of the Bagnold beach equation. *Mar. Geo.*, 61, 95–101.
Hughes, M.G., Masselink, G., Brander, R.W., 1997. Flow velocity and sediment transport in the swash zone of a steep beach. *Mar. Geol.*, 138 (1–2), 91–103.
Masselink, G., Evans, D., Hughes, M.G. & Russell, P., 2005. Suspended sediment transport in the swash zone of a dissipative beach. *Mar. Geol.*, 216, 169–189.
Masselink, G., Hughes, M., 1998. Field investigation of sediment transport in the swash zone. *Cont. Shelf Res.*, 18(10), 1179-1199.
Masselink, G., Russell, P., Turner, I.L., Blenkinsopp, C., 2009. Net sediment transport and morphological change in the swash zone of a high-energy sandy beach from swash event to tidal cycle time scales. *Mar. Geol.*, 267, 18–35.
Meyer-Peter, E., Müller, R., 1948. Formulas for bedload transport. *Proceedings 2nd Meeting of International Association for Hydraulic Research*, Stockholm, 26 pp.
Nielsen, P. 1992. *Coastal bottom boundary layers and sediment transport*. World Scientific.
O'Donoghue, T., Kikkert, G.A., Pokrajac, D., Dodd, N., Briganti, R., 2016. Intra-swash hydrodynamics and sediment flux for dambreak swash on coarse-grained beaches. *Coast. Eng.*, 112, 113–130.
Othman, I.K., Baldock, T.E., Callaghan, D.P., 2014. Measurement and modelling of the influence of grain size and pressure gradient on swash uprush sediment transport. *Coast. Eng.*, 83, 1–14.
Puleo, J. A., Beach, R. A., Holman, R. A., Allen, J. S., 2000. Swash zone sediment suspension and transport and the importance of bore-generated turbulence. *J. of Geophys. Res., Oceans*, 105(C7), 17021-17044.
Puleo, J.A., Butt, T., Plant, N.G., 2005. Instantaneous energetics sediment transport model calibration. Coast. Eng. 52, 647–653.
Puleo, J.A., Lanckriet, T.M., Wang, P., 2012. Near bed cross-shore velocity profiles, bed shear stress and friction on the foreshore of a microtidal beach, *Coast. Eng.*, 68(10), 6–16.
Raffel, M., Willert, C., Wereley, S., Kompenhans, J., 2007. *Particle Image Velocimetry-A Practical Guide*. Springer-Verlag, Berlin, Heidelberg.
Soulsby, R. L. 1997. *Dynamics of Marine Sands: A Manual for Practical Applications*. London: Thomas Telford. 249. pp.
Wu, L., Feng, D., Shimozono, T., Okayasu, A., 2014. Sediment flux measurement at high concentration based on image analysis with combined illumination. *J. JSCE*, Ser. B 70(2), 736−740.
Wu, L., Feng, D., Shimozono, T., Okayasu, A., 2016. Laboratory measurements of sediment flux and bed level evolution in the swash zone. *Coast. Eng. J.*, 58, 1650004(1-17).